Applied Mathematics & Information Sciences
An International Journal

http://dx.doi.org/10.18576/amis/200209

A New Three-Parameter Extended Pareto Distribution: Theory, Sustainable Lifetime Modeling, and Decision-Making Applications

Mohamed El-Dawoody[1], *Mahmoud El-Morshedy*[1] *and Mohamed S. Eliwa* [2,3,*]

[1]Department of Mathematics, College of Science and Humanities in Al-Kharj, Prince Sattam bin Abdulaziz University, Al-Kharj 11942, Saudi Arabia
[2]Department of Statistics and Operations Research, College of Science, Qassim University, Saudi Arabia
[3]Department of Mathematics, Faculty of Science, Mansoura University, Mansoura 35516, Egypt

Received: 20 Dec. 2025, Revised: 13 Feb. 2026, Accepted: 20 Feb 2026
Published online: 1 Mar. 2026

Abstract: This work introduces a novel three-parameter extension of the Pareto distribution, specifically examined for its utility in addressing complex data challenges within sustainability science and environmental modeling. A thorough examination of the model provides explicit formulas for properties such as the hazard rate and moments, creating a mathematical foundation for assessing sustainability risks and ecological resilience. To support social sustainability and economic equity, we utilize the Lorenz curve and Gini index to evaluate how well the distribution measures wealth inequality and fair resource allocation. The suggested model exhibits high flexibility, allowing it to accurately represent the asymmetric and leptokurtic data patterns frequently encountered in climate change studies and environmental impact assessments. Furthermore, this novel distribution is vital for the circular economy and sustainable engineering, as its flexible hazard rate function capable of modeling upside-down bathtub shapes can accurately predict product lifecycles and the reliability of green infrastructure. Maximum Likelihood Estimation (MLE) is applied to ensure precise parameter fitting, which is essential for deriving accurate sustainable development indicators. Through rigorous simulation and application to real-world datasets, we demonstrate that this model offers a superior framework for analyzing lifetime sustainability phenomena, thereby supporting more effective data-driven sustainability policies.

Keywords: Statistical model; Hazard rate function; Maximum likelihood estimation; Sustainable development; Simulation; Decision-making.

1 Introduction

For a long time, the Pareto distribution has been known to be a strong and flexible way to describe many different sustainability and environmental phenomena. Because it can show heavy-tailed behavior, it has been widely used to analyze data related to sustainable development. Reference [1] shows that the Pareto distribution is a good way to represent things like carbon emission distributions across nations, resource consumption patterns, renewable energy output variability, and other sustainability-related variables. The Pareto model has been used in many fields beyond environmental economics, such as climate risk assessment, sustainable urban planning, ecological modeling, environmental reliability analysis, and life-cycle assessment research. References [2], [3], [4], [5], [6], [7], and [8] all discuss Pareto-type models in detail and give examples of how to apply them in sustainability contexts. There has been a lot of interest in the last few years in creating exponentiated-type distributions. This is because they are very flexible and work better than other types of distributions when it comes to representing complex real-world sustainability data. These distributions have shown to be very useful in many fields, including climatology, environmental science, hydrological engineering, disaster risk modeling, environmental quality-control research, and ecological reliability analysis, as [9] points out. After that, [10] put forth the exponentiated Pareto distribution. The exponentiated Fréchet, exponentiated Weibull,

* Corresponding author e-mail: mseliwa@mans.edu.eg

© 2026 NSP
Natural Sciences Publishing Cor.

exponentiated gamma, and exponentiated Gumbel distributions are all new versions of their classical counterparts. This is similar to how the generalized exponential distribution was discussed in [10] and systematically reviewed by [11]. Other important extensions are the exponentiated generalized inverse Gaussian distribution proposed by [12], the exponentiated generalized Weibull–Gompertz distribution and its mixture model introduced by [13] and [14], and the exponentiated discrete Lindley distribution developed by [15]. These extended models offer promising tools for analyzing complex sustainability challenges, such as modeling extreme climate events, assessing the reliability of renewable energy systems, and evaluating the long-term durability of green infrastructure. Recently, a lot of research has been done on novel probability models and ways to modify them to make the analysis of sustainability-related lifetime data more flexible. For those interested, [16], [17], [18], [19], and [20] offer a thorough look at different new ways to build and expand lifetime distributions applicable to sustainable development contexts. Due to the growing complexity of sustainability data and the swift advancement of environmental monitoring and data-generating technologies, traditional probability models frequently do not sufficiently represent the underlying distributional characteristics found in practice. Modern datasets, especially those from renewable energy systems, environmental reliability analysis, green infrastructure durability, climate risk assessment, and sustainable resource management contexts, often display significant skewness, variable kurtosis levels, intricate hazard-rate patterns, heterogeneous dispersion, and the occurrence of outliers. These attributes necessitate the creation of more adaptable and resilient distributional frameworks that can accommodate the diverse data structures encountered in sustainability science. This study presents an exponentiated variant of a recently suggested Pareto distribution, termed the exponentiated new Pareto (ENP) distribution, in answer to these challenges. The exponentiation process greatly improves the baseline model's versatility by incorporating an extra shape parameter, enabling the distribution to represent various hazard rate shapes, including declining, constant, and inverted bathtub forms, which are commonly observed in the degradation patterns of sustainable technologies and ecological systems. Furthermore, the ENP distribution can describe asymmetric data exhibiting diverse kurtosis levels, from platykurtic to leptokurtic characteristics, while adeptly managing both under-dispersed and over-dispersed data structures frequently encountered in environmental and sustainability datasets. The ENP distribution offers enhanced robustness in managing datasets affected by extreme observations or outliers, which are prevalent in climate, environmental, and sustainability statistics. The enhanced modeling flexibility offered by the exponentiated structure facilitates a more precise depiction of intricate sustainability data patterns, resulting in superior inferential performance and more dependable decision-making outcomes for sustainable development planning. Thus, the suggested ENP model presents a robust and adaptable alternative to current Pareto-type distributions for contemporary sustainability data modeling applications, supporting more informed and evidence-based approaches to achieving long-term environmental, social, and economic sustainability goals.

The following portions of this document are organized as outlined below. Section 2 formally delineates the ENP distribution and elucidates its fundamental properties. Section 3 concentrates on the derivation and examination of critical structural characteristics of the proposed distribution, including its moments, related measures, and the distribution of order statistics. In Section 4, the unknown model parameters are estimated using the maximum likelihood estimation approach, and the associated inferential processes are analyzed. Section 5 discusses simulation tests to evaluate the performance of the model parameters using the maximum likelihood estimation (MLE) approach for various sample sizes. Section 6 demonstrates the practical applicability and effectiveness of the proposed ENP family by its application to an actual dataset. Section 7 offers closing insights and potential directions for future research.

2 Exponentiated New Pareto Distribution: Mathematical Theory and Visualizations

The new Pareto-type (NP) distribution was introduced by [21]. The cumulative distribution function (CDF), established for shape and scale parameters $\alpha > 0$ and $\beta > 0$, is expressed as

$$G(x;\alpha,\beta) = 1 - \frac{2\left(\frac{\beta}{x}\right)^{\alpha}}{1+\left(\frac{\beta}{x}\right)^{\alpha}};\ x \geq \beta. \tag{1}$$

The probability density function (PDF) of the NP distribution is given by

$$g(x;\alpha,\beta) = \frac{2\alpha\beta^{\alpha}x^{\alpha-1}}{(x^{\alpha}+\beta^{\alpha})^{2}};\ x \geq \beta. \tag{2}$$

The formulation of an exponentiated distribution is simple and relies on the premise that elevating an arbitrary CDF $G(x)$ to a positive exponent $\theta > 0$ produces a new CDF $F(x) = \{G(x)\}^{\theta}$, incorporating an additional shape parameter. The parameter θ regulates the skewness, kurtosis, and tail characteristics of the resultant distribution $F(x)$. Within this paradigm, $G(x)$ functions as the foundational distribution, whereas $F(x)$ is designated as the exponentiated G distribution. It is important to observe that, for $\theta > 1$ ($\theta < 1$) and for large values of x, the factor $\theta\{G(x)\}^{\theta-1}$ exceeds (falls below) one; the opposite trend occurs for smaller values of x. Thus, the

© 2026 NSP
Natural Sciences Publishing Cor.

ordinary moments linked to the density function $f(x) = \theta\{G(x)\}^{\theta-1}g(x)$ are unequivocally greater (lesser) than those pertaining to the baseline density $g(x)$ when $\theta > 1$ ($\theta < 1$). The CDF of the ENP model is given as

$$F(x;\alpha,\beta,\theta) = \left(1 - \frac{2\left(\frac{\beta}{x}\right)^{\alpha}}{1+\left(\frac{\beta}{x}\right)^{\alpha}}\right)^{\theta}; x \geq \beta. \quad (3)$$

Clearly, if $\theta = 1$, the ENP distribution reduces to the NP distribution. The ENP density function can be written as

$$f(x;\alpha,\beta,\theta) = \frac{2\theta\alpha}{\beta}\left(\frac{\beta}{x}\right)^{\alpha+1}\left(1+\left(\frac{\beta}{x}\right)^{\alpha}\right)^{-2} \times \left(1 - \frac{2\left(\frac{\beta}{x}\right)^{\alpha}}{1+\left(\frac{\beta}{x}\right)^{\alpha}}\right)^{\theta-1}, \quad x \geq \beta. \quad (4)$$

If X is a random variable with density in (4), the shorthand $X \sim \text{ENP}(\alpha,\beta,\theta)$ is used to indicate that the random variable X has the ENP distribution with parameters α, β and θ, then the survival function of X is given by

$$S(x;\alpha,\beta,\theta) = 1 - \left(1 - \frac{2\left(\frac{\beta}{x}\right)^{\alpha}}{1+\left(\frac{\beta}{x}\right)^{\alpha}}\right)^{\theta}; x \geq \beta, \quad (5)$$

and the hazard rate function (HRF) can be formulated as

$$h(x;\alpha,\beta,\theta) = \frac{2\theta\alpha\beta^{\alpha}x^{\alpha-1}\left(1 - \frac{2\left(\frac{\beta}{x}\right)^{\alpha}}{1+\left(\frac{\beta}{x}\right)^{\alpha}}\right)^{\theta-1}}{(x^{\alpha}+\beta^{\alpha})^{2}\left[1-\left(1 - \frac{2\left(\frac{\beta}{x}\right)^{\alpha}}{1+\left(\frac{\beta}{x}\right)^{\alpha}}\right)^{\theta}\right]}; x \geq \beta. \quad (6)$$

One can easily verify from (6) that the limit of the ENP hazard function as $x \to \infty$ is 0 and the limit as $x \to \beta$ are

$$\lim_{x\to\beta} h(x;\alpha,\beta,\theta) = \begin{cases} \infty, & \text{for } 0 < \theta < 1, \\ \frac{\alpha}{2\beta}, & \text{for } \theta = 1, \\ 0, & \text{for } \theta > 1. \end{cases}$$

It is possible to confirm that the suggested distribution can display both decreasing and inverted bathtub-shaped hazard rate curves, contingent upon the parameter values. Figure 1 shows how the ENP probability density function and its HRF act for several combinations of the parameters α, β, and θ. These graphs show how flexible the ENP model is when it comes to capturing different failure-rate patterns. The ENP distribution is also a good choice for modeling favorably skewed data with a unimodal form, which makes it a good choice for analyzing reliability and longevity data.

3 Statistical Properties

3.1 Quantiles and Related Statistical Measures

The qth quantile x_q of an $\text{ENP}(\alpha,\beta,\theta)$ random variable X is given by

$$x_q = Q(q;\alpha,\beta,\theta) = \beta\left[2\left(1-q^{\frac{1}{\theta}}\right)^{-1} - 1\right]^{1/\alpha}; \quad 0 < q < 1. \quad (7)$$

By definition, the $100q$th quantile is the solution of

$$q = P(X \leq x_q) = F(x_q), \quad x_q \geq \beta.$$

Substituting the CDF of the ENP distribution from (3), we have

$$q = F(x_q) = \left(1 - \frac{2\left(\frac{\beta}{x_q}\right)^{\alpha}}{1+\left(\frac{\beta}{x_q}\right)^{\alpha}}\right)^{\theta}; \quad x_q \geq \beta,$$

which can be rearranged as

$$q^{\frac{1}{\theta}} = 1 - \frac{2\beta^{\alpha}}{x_q^{\alpha}+\beta^{\alpha}} \quad \Rightarrow \quad x_q^{\alpha}+\beta^{\alpha} = 2\beta^{\alpha}\left(1-q^{\frac{1}{\theta}}\right)^{-1}$$
$$\Rightarrow \quad x_q = \beta\left[2\left(1-q^{\frac{1}{\theta}}\right)^{-1} - 1\right]^{1/\alpha}. \quad (1)$$

By setting $q = 0.25, 0.5$, and 0.75 in equation (7), one obtains the first, second (median), and third quartiles of the ENP distribution, respectively. In particular, the median corresponds to $q = 0.5$.

$$m = Q(0.5;\alpha,\beta,\theta) = \beta\left[2\left(1-\left(\frac{1}{2}\right)^{\frac{1}{\theta}}\right)^{-1} - 1\right]^{1/\alpha}. \quad (8)$$

Moreover, random samples from an $\text{ENP}(\alpha,\beta,\theta)$ distribution can be generated using the inversion method, as follows:

$$x = Q(u) = \beta\left[\frac{1+u^{\frac{1}{\theta}}}{1-u^{\frac{1}{\theta}}}\right]^{1/\alpha}; \quad 0 < u < 1. \quad (9)$$

The Bowley skewness (1962) is defined as

$$sk = \frac{Q\left(\frac{3}{4}\right)+Q\left(\frac{1}{4}\right)-2Q\left(\frac{1}{2}\right)}{Q\left(\frac{3}{4}\right)-Q\left(\frac{1}{4}\right)}, \quad (10)$$

while the Moors kurtosis is given by

$$\kappa = \frac{Q\left(\frac{3}{8}\right)-Q\left(\frac{1}{8}\right)+Q\left(\frac{7}{8}\right)-Q\left(\frac{5}{8}\right)}{Q\left(\frac{3}{4}\right)-Q\left(\frac{1}{4}\right)}. \quad (11)$$

Figure 2 illustrates the Bowley skewness and Moors kurtosis for selected parameter values, highlighting how these shape measures vary with the parameters of the ENP distribution.

© 2026 NSP
Natural Sciences Publishing Cor.

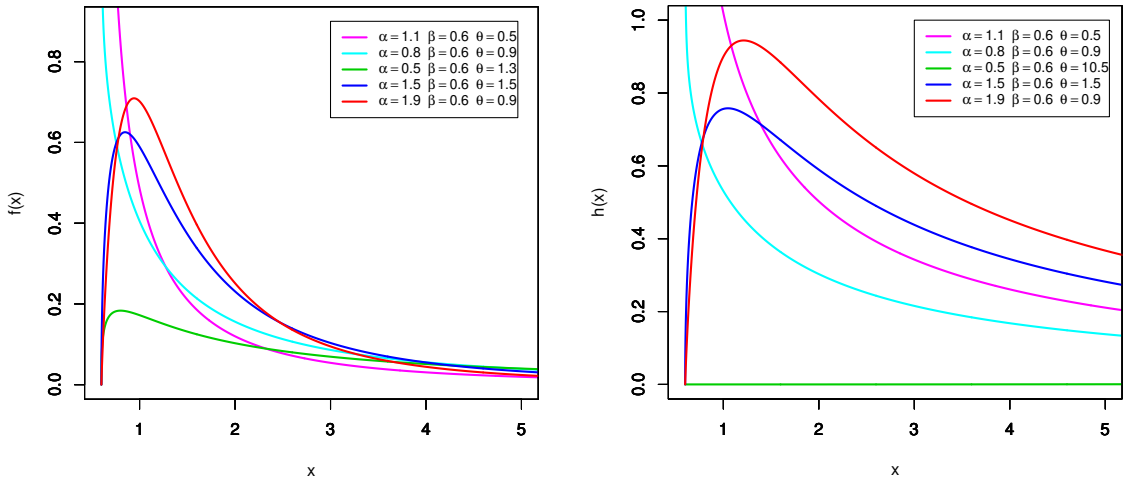

Fig. 1: The PDF and HRF plots for various values of the model parameters.

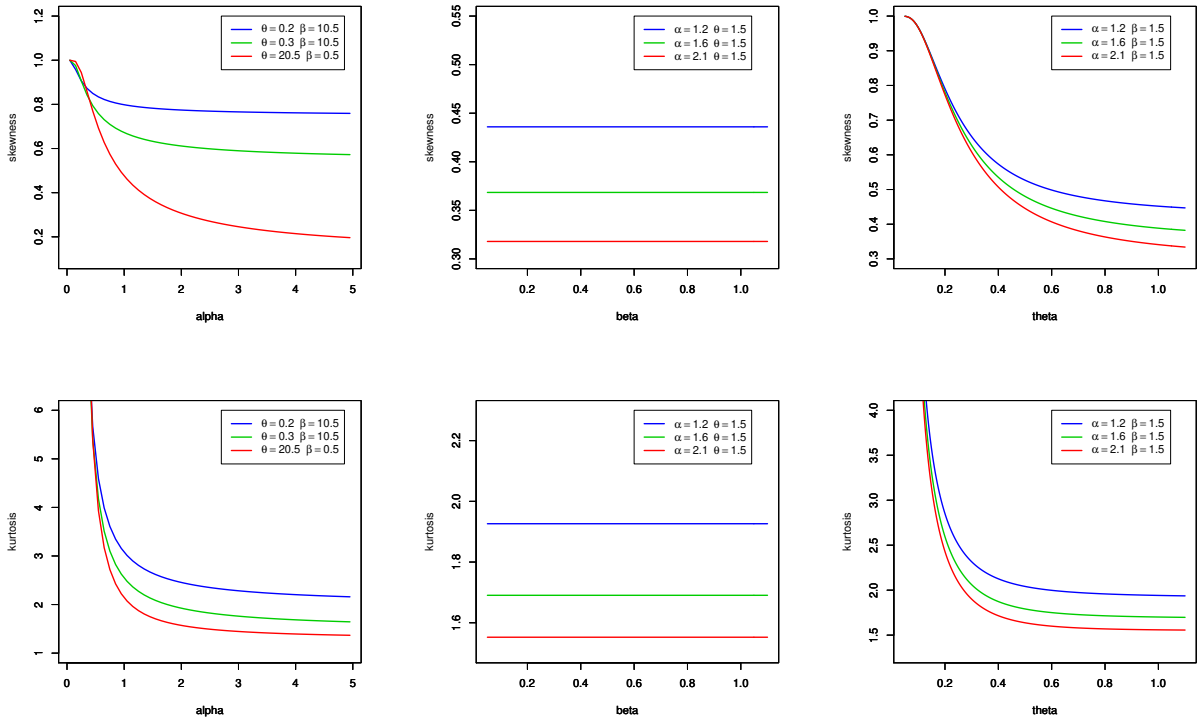

Fig. 2: The Bowley skewness and Moors kurtosis for selected values of the parameters.

© 2026 NSP
Natural Sciences Publishing Cor.

3.2 The Mode

To get the mode of ENP(α,β,θ), we first have to differentiate its PDF with respect to x to get

$$\begin{aligned} f'(x;\alpha,\beta,\theta) =& 2\theta\alpha\beta^{\alpha}x^{\alpha-1}\left(x^{\alpha}+\beta^{\alpha}\right)^{-2}\left(1-\frac{2\beta^{\alpha}}{x^{\alpha}+\beta^{\alpha}}\right)^{\theta-1} \\ &\times\left\{(\alpha-1)x^{-1}-2\alpha x^{\alpha-1}\left(x^{\alpha}+\beta^{\alpha}\right)^{-1}\right. \\ &+(\theta-1)\alpha x^{\alpha-1}\left(x^{\alpha}+\beta^{\alpha}\right)^{-2} \\ &\left.\times\left(1-\frac{2\beta^{\alpha}}{x^{\alpha}+\beta^{\alpha}}\right)^{-1}\right\} \\ =& f(x;\alpha,\beta)\left\{(\alpha-1)\frac{1}{x}-2\alpha x^{\alpha-1}\left(x^{\alpha}+\beta^{\alpha}\right)^{-1}\right. \\ &\left.+(\theta-1)\alpha x^{\alpha-1}\left(x^{2\alpha}-\beta^{2\alpha}\right)^{-1}\right\}. \end{aligned} \tag{2}$$

The mode of the distribution can be obtained by setting the first derivative of the probability density function with respect to x equal to zero. Since $f(x;\alpha,\beta,\theta)>0$, the mode is the solution of the following equation with respect to x:

$$\begin{aligned} &(\alpha-1)\frac{1}{x}-2\alpha x^{\alpha-1}\left(x^{\alpha}+\beta^{\alpha}\right)^{-1} \\ &+(\theta-1)\alpha x^{\alpha-1}\left(x^{2\alpha}-\beta^{2\alpha}\right)^{-1}=0. \end{aligned} \tag{12}$$

The nonlinear (12) does not admit a closed-form solution for x. Hence, it must be solved numerically using a suitable mathematical software package. For the NP(α,β) distribution, the mode can be obtained from (12) by setting $\theta=1$, giving

$$\text{Mode}_{\text{NP}}(x)=\beta\left(\frac{\alpha-1}{\alpha+1}\right)^{1/\alpha}.$$

3.3 Moments and Moment Generating Function

The rth raw moment of the ENP(α,β,θ) distribution, for $r=1,2,3,\ldots$, is given by

$$\begin{aligned} \mu_r' =& 2\theta\beta^r\frac{\Gamma\left(1-\frac{r}{\alpha}\right)\Gamma(\theta)}{\Gamma\left(1-\frac{r}{\alpha}+\theta\right)} \\ &\times{}_2F_1\left(\theta+1,\,1-\frac{r}{\alpha},\,\theta+1-\frac{r}{\alpha},\,-1\right), \quad r<\alpha, \end{aligned} \tag{13}$$

where ${}_2F_1(\cdot)$ denotes the hypergeometric function. By definition, the rth raw moment of a random variable X with PDF $f(x;\alpha,\beta,\theta)$ is

$$\mu_r'=\mathbb{E}[X^r]=\int_{-\infty}^{\infty}x^r f(x;\alpha,\beta,\theta)\,dx.$$

Substituting the ENP PDF from (4) gives

$$\mu_r'=2\theta\alpha\int_{\beta}^{\infty}x^r\frac{\left(\frac{\beta}{x}\right)^{\alpha+1}}{\beta\left[1+\left(\frac{\beta}{x}\right)^{\alpha}\right]^2}\left[1-\frac{2\left(\frac{\beta}{x}\right)^{\alpha}}{1+\left(\frac{\beta}{x}\right)^{\alpha}}\right]^{\theta-1}dx.$$

Letting $t=\left(\frac{\beta}{x}\right)^{\alpha}$ transforms the integral into

$$\mu_r'=2\theta\beta^r\int_0^1 t^{-r/\alpha}(1-t)^{\theta-1}(1+t)^{-(\theta+1)}\,dt. \tag{14}$$

Using the integral representation of the hypergeometric function

$${}_2F_1(a,b,c,z)=\frac{\Gamma(c)}{\Gamma(b)\Gamma(c-b)}\int_0^1 t^{b-1}(1-t)^{c-b-1}(1-zt)^{-a}\,dt, \tag{15}$$

we recover the expression in (13), completing the proof. From the raw moments, standard statistical measures can be derived. The mean, variance, coefficient of variation, skewness, and kurtosis of the ENP distribution are given by

$$\begin{aligned} \mu_1' =& \frac{2\theta\beta\Gamma\left(1-\frac{1}{\alpha}\right)\Gamma(\theta)}{\Gamma\left(1-\frac{1}{\alpha}+\theta\right)} \\ &\times{}_2F_1\left(\theta+1,1-\frac{1}{\alpha},\theta+1-\frac{1}{\alpha},-1\right), \quad \alpha>1, \end{aligned} \tag{16}$$

$$\sigma^2=\mu_2'-\mu_1'^2, \tag{17}$$

$$cv=\frac{\sigma}{\mu_1'}=\sqrt{\frac{\mu_2'}{\mu_1'^2}-1}, \tag{18}$$

$$sk=\frac{\mathbb{E}[(X-\mu_1')^3]}{\sigma^3}=\frac{\mu_3'-3\mu_1'\mu_2'+2\mu_1'^3}{(\mu_2'-\mu_1'^2)^{3/2}}, \tag{19}$$

$$\kappa=\frac{\mathbb{E}[(X-\mu_1')^4]}{\sigma^4}=\frac{\mu_4'-4\mu_1'\mu_3'+6\mu_1'^2\mu_2'-3\mu_1'^4}{(\mu_2'-\mu_1'^2)^2}, \tag{20}$$

where μ_1',μ_2',μ_3', and μ_4' are obtained from (13) by setting $r=1,2,3,4$, respectively. The moment generating function (MGF) of the ENP distribution can be obtained from its rth raw moment, expressed as:

$$\begin{aligned} E\left(e^{tx}\right) =& \sum_{i=0}^{\infty}\frac{t^i}{i!}E\left(X^i\right) \\ =& \sum_{i=0}^{\infty}\frac{t^i}{i!}\frac{\Gamma\left(1-\frac{i}{\alpha}\right)\Gamma(\theta)}{\Gamma\left(1-\frac{i}{\alpha}+\theta\right)} \\ &\times{}_2F_1\left[\theta+1,\,1-\tfrac{i}{\alpha},\,\theta+1-\tfrac{i}{\alpha},\,-1\right]; \quad i<\alpha, \end{aligned} \tag{21}$$

Table 1 presents the mean, variance, skewness, kurtosis, and dispersion index of the ENP distribution for various combinations of the parameters α, β, and θ.

According to Table 2, it can be observed that

–The mean increases with both β and θ, reflecting their roles as scale and shape parameters. For example, Scheme 2 ($\beta=2,\theta=1$) has a higher mean (2.574) compared to Scheme 1 ($\beta=1,\theta=0.5$, mean = 1.197). This indicates that the distribution can be adjusted to have a higher central tendency by increasing β or θ.

© 2026 NSP
Natural Sciences Publishing Cor.

Table 1: Statistical properties of the distribution for selected parameter schemes.

Scheme	α	β	θ	Mean	Variance	Skewness	Kurtosis	Index of Dispersion
1	5.5	1.0	0.5	1.197	0.081	4.103	47.803	0.067
2	6.0	2.0	1.0	2.574	0.364	3.201	29.132	0.142
3	6.5	1.5	0.8	1.837	0.145	3.121	25.669	0.079
4	7.0	0.8	1.2	1.013	0.040	2.721	20.019	0.040
5	7.5	1.0	0.7	1.173	0.041	2.914	20.796	0.035
6	8.0	1.2	0.6	1.373	0.045	2.932	20.171	0.033
7	8.5	2.0	1.5	2.480	0.159	2.311	14.418	0.064
8	9.0	1.0	1.0	1.177	0.029	2.410	14.697	0.025
9	9.5	1.8	0.9	2.080	0.079	2.406	14.317	0.038
10	10.0	2.0	1.1	2.333	0.093	2.244	12.914	0.040

–Variance is generally low for schemes with moderate β and higher α, indicating the distribution is concentrated around the mean. Higher β (e.g., Schemes 2, 7, and 10) increases variance significantly, showing greater dispersion. Variance is influenced less strongly by α than by β and θ.
–All schemes exhibit positive skewness, indicating right-skewed distributions. Skewness decreases with higher α and higher θ, suggesting that increasing these parameters produces a more symmetric distribution. For instance, Scheme 1 ($\alpha = 5.5, \theta = 0.5$) has high skewness (4.103), whereas Scheme 10 ($\alpha = 10, \theta = 1.1$) has moderate skewness (2.244).
–Kurtosis is extremely high for schemes with small α and low θ, indicating heavy tails and higher probability of extreme values. As α and θ increase, kurtosis decreases substantially (e.g., Scheme 10 has 12.914), implying thinner tails and less likelihood of outliers.
–All schemes have index of dispersion (ID = Variance / Mean) less than 1, showing underdispersion (variance smaller than mean). This indicates the distribution is concentrated and exhibits low variability relative to the mean. The lowest ID occurs in schemes with small variance and moderate mean (e.g., Scheme 8, ID = 0.025).

An elevation in α typically results in a decrease in skewness and kurtosis, yielding a distribution with lighter tails. Elevated values of β predominantly amplify the distribution, resulting in proportional increases in both the mean and variance. Augmenting θ generally reduces skewness and kurtosis, so concentrating the probability mass around the mean. The distribution exhibits significant flexibility; by suitably modifying α, β, and θ, it can represent a diverse array of behaviors, ranging from markedly skewed and heavy-tailed to moderately symmetric and concentrated. This adaptability renders it especially appropriate for modeling datasets where skewness, tail behavior, or underdispersion are critical factors.

3.4 Lorenz Curve and Gini Index: Theory and Computation

Lorenz curves have numerous applications, not only in economics to study income and poverty, but also in fields such as reliability, demography, insurance, and medicine. For a PDF $f(x;.)$ with CDF $F(x;.)$, the Lorenz curve $L(p)$ is defined as

$$L(p) = \frac{\int_{-\infty}^{q} t f(t)\,dt}{\int_{-\infty}^{\infty} t f(t)\,dt} = \frac{\int_{-\infty}^{q} t f(t)\,dt}{\mu}, \tag{22}$$

where μ denotes the mean and $q = F_{\text{ENP}}^{-1}(p)$ is the quantile function of X. For the ENP distribution, the Lorenz curve can be expressed as

$$\begin{aligned} L(p) &= \frac{\int_{\beta}^{q} t f(t)\,dt}{\mu} = \frac{1}{\mu}\left[\int_{\beta}^{\infty} x f(x)\,dx - \int_{q}^{\infty} x f(x)\,dx\right] \\ &= \frac{1}{\mu}\left[\mu - \frac{2\theta q \Gamma\left(1-\frac{1}{\alpha}\right)\Gamma(\theta)}{\Gamma\left(1-\frac{1}{\alpha}+\theta\right)}\right. \\ &\qquad \left. \times {}_2F_1\left(\theta+1,\, 1-\tfrac{1}{\alpha},\, 1-\tfrac{1}{\alpha}+\theta,\, -1\right)\right]. \end{aligned} \tag{23}$$

The Lorenz curve also allows us to define the Gini coefficient, a widely used measure of inequality. It is computed as twice the area between the Lorenz curve and the egalitarian line. The Gini coefficient ranges between 0 and 1, with 0 representing perfect equality and 1 representing perfect inequality. It is widely used in contexts such as energy, credit availability, income, health care, and wealth (see, [22]). For the ENP distribution, the

© 2026 NSP
Natural Sciences Publishing Cor.

Gini coefficient is given by

$$\text{Gini} = 1 - 2\int_0^1 L(p)\,dp = 1 - \frac{2\int_0^1\int_0^p q(t)\,dt\,dp}{\mu}$$
$$= 1 - \frac{\Gamma\left(1-\frac{1}{\alpha}+\theta\right)}{\theta\,\Gamma\left(1-\frac{1}{\alpha}\right)\Gamma(\theta)} \times \frac{1}{{}_2F_1\left(\theta+1,\,1-\frac{1}{\alpha},\,1-\frac{1}{\alpha}+\theta,\,-1\right)} \times \int_0^1\int_0^p \left[\frac{1+t^{1/\theta}}{1-t^{1/\theta}}\right]^{1/\alpha} dt\,dp. \tag{24}$$

A comprehensive algebraic treatment of the Gini index can be found in [23]. To illustrate the behavior of the ENP distribution, we consider three combinations of parameters (α,β,θ) and compute the Lorenz curve at selected percentiles $p = 0.25, 0.5, 0.75$, along with the Gini index. The results are summarized in Table 2. The Lorenz curves $L(p)$ show how much of the variable (such income or lifetime) is made up of the poorest p percent of the population. When p is the same, lower values of $L(p)$ mean more inequality. The Gini index, which measures inequality, goes up when the distribution is more uneven or focused. For example, combination 2 with $(\alpha,\beta,\theta) = (1.5,1,2)$ has the highest Gini index of 0.34, which means that the other parameter sets have less inequality. As seen in combination 3, larger values of α or smaller values of θ tend to lower skewness, which leads to lower Gini indices. These calculations show how ENP factors affect measurements of inequality, showing how important they are in domains like economics, reliability, and health sciences.

3.5 Order Statistics

Order statistics are used to find the characteristics such as minimum and maximum time to failure of electronic components for example lightbulbs in reliability theory. This may be achieved by testing n lightbulbs and simultaneously putting them on test and collecting the time to failure as the successive failures occur.

Theorem 1. The PDF of the ith order statistic fron ENP distribution can be formulated as

$$f_{i:n}(x;\Theta) = \frac{2\alpha\beta^\alpha(n!)}{(n-i)!\,(i-1)!}\sum_{j=0}^{\infty}\sum_{k=0}^{\infty}(-1)^{j+k}\binom{n-i}{j}\binom{\theta-1}{j} \times \frac{x^{\alpha-1}}{(x^\alpha+\beta^\alpha)^2}\left[\frac{2\beta^\alpha}{x^\alpha+\beta^\alpha}\right]^{i+j+k-1}. \tag{25}$$

Proof. Let $X_1, X_2, \ldots, X_n$ denote a random sample drawn from a population with PDF $f(x;\cdot)$ and CDF $F(x;\cdot)$. The PDF of the ith order statistic is given as

$$f_{i:n}(x;\Theta) = \frac{n!}{n-i!i-1!} f(x;\Theta)\,[F(x;\Theta)]^{i-1}\,[1-F(x;\Theta)]^{n-i}.$$

Using the identity

$$(1-z)^{a-1} = \sum_{j=0}^{\infty}(-1)^j\binom{a-1}{j}z^j,$$

we have

$$f_{i:n}(x;\Theta) = \frac{n!\,f(x;\Theta)}{(n-i)!\,(i-1)!}\sum_{j=0}^{\infty}(-1)^j\binom{n-i}{j}[F(x;\Theta)]^{i+j-1}$$
$$= \frac{2\alpha\beta^\alpha(n!)}{(n-i)!\,(i-1)!}\sum_{j=0}^{\infty}(-1)^j\binom{n-i}{j}\frac{x^{\alpha-1}}{(x^\alpha+\beta^\alpha)^2} \times \left(1-\frac{2\beta^\alpha}{x^\alpha+\beta^\alpha}\right)^{\theta-1}\left[\frac{2\beta^\alpha}{x^\alpha+\beta^\alpha}\right]^{i+j-1}$$
$$= \frac{2\alpha\beta^\alpha(n!)}{(n-i)!\,(i-1)!}\sum_{j=0}^{\infty}\sum_{k=0}^{\infty}(-1)^{j+k}\binom{n-i}{j}\binom{\theta-1}{j} \times \frac{x^{\alpha-1}}{(x^\alpha+\beta^\alpha)^2}\left[\frac{2\beta^\alpha}{x^\alpha+\beta^\alpha}\right]^{i+j+k-1}.$$

Which completes the proof.

Theorem 2. The rth moment of the distribution of the ith order statistic is given by

$$E(X_{i:n}^r) = \frac{2\beta^r(n!)}{(n-i)!\,(i-1)!}\sum_{j=0}^{\infty}\sum_{k=0}^{\infty}(-1)^{j+k}2^{i+j+k-1} \times \binom{n-i}{j}\binom{\theta-1}{j} \times \frac{\Gamma\left(i+j+k-\frac{r}{\alpha}\right)\Gamma(1)}{\Gamma\left(i+j+k-\frac{r}{\alpha}+1\right)} \times {}_2F_1\left(i+j+k+1,\,i+j+k-\tfrac{r}{\alpha},\,i+j+k-\tfrac{r}{\alpha}+1,\,-1\right), \quad r<\alpha. \tag{26}$$

$$E(X_{i:n}^r) = \frac{2\alpha\beta^\alpha(n!)}{(n-i)!\,(i-1)!}\sum_{j=0}^{\infty}\sum_{k=0}^{\infty}(-1)^{j+k}\binom{n-i}{j}\binom{\theta-1}{j} \times \int_\beta^\infty \frac{x^{r+\alpha-1}}{(x^\alpha+\beta^\alpha)^2}\left[\frac{2\beta^\alpha}{x^\alpha+\beta^\alpha}\right]^{i+j+k-1}dx$$
$$= \frac{2\alpha(n!)}{(n-i)!\,(i-1)!}\sum_{j=0}^{\infty}\sum_{k=0}^{\infty}(-1)^{j+k}\binom{n-i}{j}\binom{\theta-1}{j} \times \int_\beta^\infty \frac{x^{r-1}\left(\frac{\beta}{x}\right)^\alpha}{\left(1+\left(\frac{\beta}{x}\right)^\alpha\right)^2}\left[\frac{2\left(\frac{\beta}{x}\right)^\alpha}{1+\left(\frac{\beta}{x}\right)^\alpha}\right]^{i+j+k-1}dx$$
$$= \frac{2\beta^r(n!)}{(n-i)!\,(i-1)!}\sum_{j=0}^{\infty}\sum_{k=0}^{\infty}(-1)^{j+k}\binom{n-i}{j}\binom{\theta-1}{j} \times \int_0^1 \frac{t^{-\frac{r}{\alpha}}}{(1+t)^2}\left[\frac{2t}{1+t}\right]^{i+j+k-1}dt$$
$$= \frac{2\beta^r(n!)}{(n-i)!\,(i-1)!}\sum_{j=0}^{\infty}\sum_{k=0}^{\infty}(-1)^{j+k}2^{i+j+k-1} \times \binom{n-i}{j}\binom{\theta-1}{j}\int_0^1 t^{i+j+k-\frac{r}{\alpha}-1}(1+t)^{-(i+j+k+1)}dt$$
$$= \frac{2\beta^r(n!)}{(n-i)!\,(i-1)!}\sum_{j=0}^{\infty}\sum_{k=0}^{\infty}(-1)^{j+k}2^{i+j+k-1}\binom{n-i}{j}\binom{\theta-1}{j} \times \frac{\Gamma\left(i+j+k-\frac{r}{\alpha}\right)\Gamma(1)}{\Gamma\left(i+j+k-\frac{r}{\alpha}+1\right)} \times {}_2F_1\left(i+j+k+1,\,i+j+k-\tfrac{r}{\alpha},\,i+j+k-\tfrac{r}{\alpha}+1,\,-1\right), \quad r<\alpha.$$

© 2026 NSP
Natural Sciences Publishing Cor.

Table 2: Lorenz curve values and Gini indices for selected ENP parameter combinations.

Combination	(α,β,θ)	$L(0.25)$	$L(0.5)$	$L(0.75)$	Gini
1	(2, 1, 1)	0.18	0.44	0.72	0.32
2	(1.5, 1, 2)	0.15	0.42	0.75	0.34
3	(3, 2, 1.5)	0.20	0.46	0.70	0.30

Which completes the proof.

Theorem 3. Let $Y = min\{X_1, X_2, ..., X_n\}$. The density function of the minimum of n independent ENP random variables is

$$f_Y(y) = \frac{2n\alpha\theta\beta^\alpha y^{\alpha-1}}{(y^\alpha+\beta^\alpha)^2}\left(1-\frac{2\beta^\alpha}{y^\alpha+\beta^\alpha}\right)^{\theta-1} \times\left[1-\left(1-\frac{2\beta^\alpha}{y^\alpha+\beta^\alpha}\right)^{\theta}\right]^{n-1}. \quad (27)$$

Proof.

$$\begin{aligned} F_Y(y) &= P(Y \le y) \\ &= 1 - P(\min\{X_1, X_2, \ldots, X_n\} \ge y) \\ &= 1 - P(X_1 \ge y)\,P(X_2 \ge y)\cdots P(X_n \ge y) \\ &= 1 - \left[1-\left(1-\frac{2\beta^\alpha}{y^\alpha+\beta^\alpha}\right)^{\theta}\right]^n. \end{aligned}$$

Thus, the PDF of Y is given by

$$f_Y(y) = \frac{2n\alpha\theta\beta^\alpha y^{\alpha-1}}{(y^\alpha+\beta^\alpha)^2}\left(1-\frac{2\beta^\alpha}{y^\alpha+\beta^\alpha}\right)^{\theta-1} \times\left[1-\left(1-\frac{2\beta^\alpha}{y^\alpha+\beta^\alpha}\right)^{\theta}\right]^{n-1}.$$

4 Maximum Likelihood Estimation and Information Matrix

In this section, we derive the maximum likelihood estimates (MLEs) for the three parameters α, β, and θ. Subsequently, we obtain the Fisher information matrix and construct the confidence intervals for the model parameters. Let $x_1, \ldots, x_n$ denote a random sample of size n drawn from the ENP distribution. The likelihood function, L, for the ENP distribution is given as

$$L = \prod_{i=1}^{n} \frac{2\theta\alpha\beta^\alpha x_i^{\alpha-1}}{(x_i^\alpha+\beta^\alpha)^2}\left(1-\frac{2\beta^\alpha}{x_i^\alpha+\beta^\alpha}\right)^{\theta-1}; x \ge \beta. \quad (28)$$

The maximum likelihood estimates for α, β and θ are the values of α, β and θ that make L as large as possible given the data we have. The most familiar method of maximizing functions involves calculus. However, we need no calculus to see that L gets large beyond bound for increases in β. It is key then to recall that β can be no larger than the smallest value of x in our data, so the best we can do in maximizing L by adjusting β is as follows:

$$\hat{\beta} = \min\{x_i\} = x_{(1)}. \quad (29)$$

In order to find the maximum likelihood estimate for α and θ, calculus is appropriate. Since L is nonnegative, we can take its logarithm. We do this because it is easier to differentiate $\log L$ than L itself. The loglikelihood function is then given by:

$$\begin{aligned} \ell(\alpha,\beta,\theta \mid x) \propto\; & n\log\alpha - n\log\beta + n\log\theta \\ & + (\alpha+1)\sum_{i=1}^{n}\log\left(\frac{\beta}{x_i}\right) \\ & - 2\sum_{i=1}^{n}\log\left(1+\left(\frac{\beta}{x_i}\right)^\alpha\right) \\ & + (\theta-1)\sum_{i=1}^{n}\log\left[1-\frac{2\left(\frac{\beta}{x_i}\right)^\alpha}{1+\left(\frac{\beta}{x_i}\right)^\alpha}\right]. \end{aligned} \quad (30)$$

To obtain the normal equations for the unknown parameters, we differentiate (30) partially with respect to α and λ and equate to zero. The resulting equations are

$$\begin{aligned} \frac{\partial\ell(\alpha,\beta,\theta \mid x)}{\partial\alpha} = & \frac{n}{\alpha} + \sum_{i=1}^{n}\log\left(\frac{\beta}{x_i}\right) \\ & - 2\sum_{i=1}^{n}\frac{\left(\frac{\beta}{x_i}\right)^\alpha\log\left(\frac{\beta}{x_i}\right)}{1+\left(\frac{\beta}{x_i}\right)^\alpha} \\ & + (\theta-1)\sum_{i=1}^{n}\frac{2\left(\frac{\beta}{x_i}\right)^\alpha\log\left(\frac{\beta}{x_i}\right)}{1-\left(\frac{\beta}{x_i}\right)^{2\alpha}}. \end{aligned} \quad (31)$$

and

$$\frac{\partial\ell(\alpha,\beta,\theta|x)}{\partial\theta} = \frac{n}{\theta} + \sum_{i=1}^{n}\log\left[1-\frac{2\left(\frac{\beta}{x_i}\right)^\alpha}{1+\left(\frac{\beta}{x_i}\right)^\alpha}\right]. \quad (32)$$

From Equation (32) we observe that

$$\hat{\theta} = -\frac{n}{\sum_{i=1}^{n}\log\left[1-\frac{2\left(\frac{x_1}{x_i}\right)^\alpha}{1+\left(\frac{x_1}{x_i}\right)^\alpha}\right]}. \quad (33)$$

© 2026 NSP
Natural Sciences Publishing Cor.

Now, on substituting the value of θ from (32) in (30), $\hat{\alpha}$ can be obtained as the solution of the following non-linear equation

$$h(\alpha) = \frac{n}{\alpha} + \sum_{i=1}^{n} \log\left(\frac{x_1}{x_i}\right)^{\alpha} - 2\sum_{i=1}^{n} \frac{\left(\frac{x_1}{x_i}\right)^{\alpha} \log\left(\frac{x_1}{x_i}\right)}{1+\left(\frac{x_1}{x_i}\right)^{\alpha}} - \left(\frac{n}{A(\alpha)}+1\right) \times \sum_{i=1}^{n} \frac{2\left(\frac{x_1}{x_i}\right)^{\alpha} \log\left(\frac{x_1}{x_i}\right)}{1-\left(\frac{x_1}{x_i}\right)^{2\alpha}}, \tag{34}$$

$$\text{where} \quad A(\alpha) = \sum_{i=1}^{n} \log\left[1 - \frac{2\left(\frac{x_1}{x_i}\right)^{\alpha}}{1+\left(\frac{x_1}{x_i}\right)^{\alpha}}\right].$$

Therefore, $\hat{\alpha}$ can be obtained as a solution of the non-linear equation of the form

$$g(\alpha) = \alpha, \tag{35}$$

where

$$g(\alpha) = n\left[-A(\alpha) + 2B(\alpha) + C(\alpha)\cdot D(\alpha)\right]^{-1}, \tag{36}$$

$$A(\alpha) = \sum_{i=1}^{n} \log\left(\frac{x_1}{x_i}\right)^{\alpha},$$

$$B(\alpha) = \sum_{i=1}^{n} \frac{\left(\frac{x_1}{x_i}\right)^{\alpha} \log\left(\frac{x_1}{x_i}\right)}{1+\left(\frac{x_1}{x_i}\right)^{\alpha}},$$

$$\text{where} \quad C(\alpha) = \frac{n}{\sum_{i=1}^{n} \log\left[1 - \frac{2\left(\frac{x_1}{x_i}\right)^{\alpha}}{1+\left(\frac{x_1}{x_i}\right)^{\alpha}}\right]} + 1,$$

$$D(\alpha) = \sum_{i=1}^{n} \frac{2\left(\frac{x_1}{x_i}\right)^{\alpha} \log\left(\frac{x_1}{x_i}\right)}{1-\left(\frac{x_1}{x_i}\right)^{2\alpha}}.$$

Since, $\hat{\alpha}$ is a fixed point solution of the non-linear equation (36), therefore, it can be obtained using an iterative scheme as follows:

$$g(\alpha_{(j)}) = \alpha_{(j+1)}, \tag{37}$$

where $\alpha_{(j)}$ is the jth iterate of $\hat{\alpha}$. The iteration procedure should be stopped when $\left|\alpha_{(j)} - \alpha_{(j+1)}\right|$ is sufficiently small. Once we obtain $\hat{\alpha}$, then $\hat{\theta}$ can be obtained from (33).

4.1 Asymptotic confidence intervals

Besides, the point estimates of the parameters, it is also desirable to have the confidence intervals for the parameters. The exact solution for the confidence intervals is not possible since the distributions of MLEs are not explicitly defined here. The asymptotic confidence intervals (CIs) are developed on the basis of asymptotic normality of the MLEs. In particular $\hat{\Theta} = \left(\hat{\alpha}, \hat{\beta}, \hat{\theta}\right)^T$ has an asymptotic normal distribution with mean $\Theta = (\alpha, \beta, \theta)^T$ and the covariance matrix determined by the Fisher information matrix. We have

$$\sqrt{n}\left(\hat{\Theta} - \Theta\right) \xrightarrow{d} N\left(0, I^{-1}(\Theta)\right), \tag{38}$$

where $\xrightarrow{d}$ denotes convergence in distribution, $I(\Theta)$ is the expected Fisher information matrix of Θ in a single observation. Note that to construct CI for Θ, the $I_n(\Theta) = nI(\Theta)$ needs to be estimated. One such approximation is the matrix $M(\Theta)$ called the empirical Fisher information matrix, see [24]. Let $\ell(\Theta)$ represent the individual case log-likelihood and

$$G_i(\Theta) = \frac{\partial \ell(\Theta)}{\partial \Theta} = \left(A(x_i, \alpha, \beta, \theta),\, B(x_i, \alpha, \beta, \theta),\, C(x_i, \alpha, \beta, \theta)\right)^T, \tag{39}$$

where

$$A(x_i, \alpha, \beta, \theta) = \frac{\partial \ell(\Theta)}{\partial \alpha} = \frac{1}{\alpha} + \log\left(\frac{\beta}{x_i}\right)^{\alpha} - \frac{2\left(\frac{\beta}{x_i}\right)^{\alpha} \log\left(\frac{\beta}{x_i}\right)}{1+\left(\frac{\beta}{x_i}\right)^{\alpha}} + 2(\theta-1)\frac{\left(\frac{\beta}{x_i}\right)^{\alpha} \log\left(\frac{\beta}{x_i}\right)}{1-\left(\frac{\beta}{x_i}\right)^{2\alpha}}. \tag{40}$$

$$B(x_i, \alpha, \beta, \theta) = \frac{\partial \ell(\Theta)}{\partial \beta} = \frac{\alpha}{\beta}\left[1 - \frac{2\left(\frac{\beta}{x_i}\right)^{\alpha}}{1+\left(\frac{\beta}{x_i}\right)^{\alpha}} - \frac{2(\theta-1)\left(\frac{\beta}{x_i}\right)^{\alpha}}{1-\left(\frac{\beta}{x_i}\right)^{2\alpha}}\right]. \tag{41}$$

and

$$C(x_i, \alpha, \beta, \theta) = \frac{\partial \ell(\Theta)}{\partial \theta} = \frac{1}{\theta} + \sum_{i=1}^{n} \log\left[1 - \frac{2\left(\frac{\beta}{x_i}\right)^{\alpha}}{1+\left(\frac{\beta}{x_i}\right)^{\alpha}}\right]. \tag{42}$$

© 2026 NSP
Natural Sciences Publishing Cor.

Then, the corresponding vector of score functions is given by

$$M(\Theta)=\sum_{i=1}^{n}G_iG_i^T-\frac{1}{n}\sum_{i=1}^{n}G_i\sum_{i=1}^{n}G_i^T. \tag{43}$$

The use of $M\left(\hat{\Theta}\right)$ as a consistent estimator of $I_n(\Theta)$ has been suggested by [25] and [26]. The diagonal elements of $M^{-1}\left(\hat{\Theta}\right)$ provides the asymptotic variances for the parameters α, β and θ respectively. Therefore, the asymptotic $100(1-\gamma)\%$ normal approximation CIs of α, β and θ can be obtaineds as

$$\left(\hat{\alpha}\pm z_{\gamma/2}\widehat{se}(\hat{\alpha})\right),\left(\hat{\beta}\pm z_{\gamma/2}\widehat{se}(\hat{\beta})\right)\text{ and }\left(\hat{\theta}\pm z_{\gamma/2}\widehat{se}(\hat{\theta})\right), \tag{44}$$

where $\widehat{se}(\cdot)$ is the square root of the diagonal element of $M^{-1}\left(\hat{\Theta}\right)$ corresponding to each parameter, and $z_{\gamma/2}$ is the quantile $100(1-\gamma/2)\%$ of the standard normal distribution. Also, we can use log transformation to obtain an approximate CI for Θ. Based on the normal approximation of the log transformed MLE, we can say that $[\log(\hat{\Theta})-\log(\Theta)]/\sqrt{Var(\log(\hat{\Theta}))}$ is asymptotically normally distributed with standard normal distribution, i.e.

$$\frac{\log(\hat{\Theta})-\log(\Theta)}{\sqrt{Var(\log(\hat{\Theta}))}}\backsim N(0,1). \tag{45}$$

If we replace the variance $Var(\log(\hat{\Theta}))\approx Var(\hat{\Theta})/\hat{\Theta}^2$ by its estimate, we can obtain a $100(1-\gamma)\%CI$ for Θ obtained as

$$\left(\hat{\Theta}\exp\left[-z_{\gamma/2}\frac{\sqrt{Var(\hat{\Theta})}}{\hat{\Theta}}\right],\ \hat{\Theta}\exp\left[z_{\gamma/2}\frac{\sqrt{Var(\hat{\Theta})}}{\hat{\Theta}}\right]\right),\quad \Theta=(\alpha,\beta,\theta). \tag{46}$$

Furthermore, applying the usual large sample approximation (assuming β to be known), the maximum likelihood estimators of α and θ can be treated as being approximately bivariate normal with mean α and θ and variance-covariance matrix equal to the inverse of the expected information matrix. Under this property, the asymptotic sampling distribution of $\begin{pmatrix}\hat{\alpha}-\alpha\\ \hat{\theta}-\theta\end{pmatrix}$ is $N_2(0,\Delta^{-1})$, where, Δ is the observed Fisher information matrix and which is defined as follows:

$$\Delta=\begin{pmatrix}-\frac{\partial^2\ell}{\partial\alpha^2} & -\frac{\partial^2\ell}{\partial\alpha\partial\theta}\\ -\frac{\partial^2\ell}{\partial\theta\partial\alpha} & -\frac{\partial^2\ell}{\partial\theta^2}\end{pmatrix}_{(\hat{\alpha},\hat{\theta})}, \tag{47}$$

where

$$\begin{aligned}\frac{\partial^2\ell}{\partial\alpha^2}=&-\frac{n}{\alpha^2}+\sum_{i=1}^{n}\log\left(\frac{x_1}{x_i}\right)\\&-2\sum_{i=1}^{n}\frac{\left(\frac{x_1}{x_i}\right)^{\alpha}\log^2\left(\frac{x_1}{x_i}\right)}{\left(1+\left(\frac{x_1}{x_i}\right)^{\alpha}\right)^2}\\&+2(\theta-1)\sum_{i=1}^{n}\left(\frac{x_1}{x_i}\right)^{\alpha}\log^2\left(\frac{x_1}{x_i}\right)\\&\times\frac{1+\left(\frac{x_1}{x_i}\right)^{2\alpha}}{\left[1-\left(\frac{x_1}{x_i}\right)^{2\alpha}\right]^2}.\end{aligned} \tag{48}$$

$$\frac{\partial\ell(\alpha,\beta,\theta|x)}{\partial\theta\partial\alpha}=\sum_{i=1}^{n}\frac{2\left(\frac{x_1}{x_i}\right)^{\alpha}\log\left(\frac{x_1}{x_i}\right)}{\left[1-\left(\frac{x_1}{x_i}\right)^{2\alpha}\right]}\text{ and }\frac{\partial^2\ell}{\partial\theta^2}=\frac{-n}{\theta^2}. \tag{49}$$

The diagonal elements of Δ^{-1} provides the asymptotic variances for the parameters α and θ respectively. Then two-sided $100(1-\gamma)\%$ normal approximation confidence interval of α and θ can be obtaineds as

$$\left(\hat{\alpha}\pm z_{\gamma/2}\widehat{se}(\hat{\alpha})\right)\text{ and }\left(\hat{\theta}\pm z_{\gamma/2}\widehat{se}(\hat{\theta})\right). \tag{50}$$

5 Simulation Analysis of Estimator Performance

In this section, we investigate the performance of the maximum likelihood estimators (MLEs) of the model parameters (α,β,θ) of the proposed distribution using the R software package. The simulation aims to examine the behavior of the estimators under various sample sizes and different parameter combinations. The simulation study is conducted according to the following steps. We consider three parameter combinations for (α,β,θ) as follows: Scheme 1: $(\alpha,\beta,\theta)=(1.5,1.0,2.0)$; Scheme 2: $(\alpha,\beta,\theta)=(2.0,1.5,1.5)$; and Scheme 3: $(\alpha,\beta,\theta)=(0.8,0.5,1.2)$. Sample sizes are taken from $n=40$ to 800 in steps of 75 where $n=40,115,190,265,340,415,490,565,640,715,790$. The step size of 75 in the simulation study was chosen to balance computational feasibility with coverage of a wide range of sample sizes. For each combination of parameters and sample size:

1. Generate n random samples from the proposed distribution using the inverse transform method.
2. Estimate the parameters $(\hat{\alpha},\hat{\beta},\hat{\theta})$ via maximum likelihood.
3. Compute 95% confidence intervals for each parameter using the asymptotic normality of the MLEs.

© 2026 NSP
Natural Sciences Publishing Cor.

4.Repeat the simulation 1000 times to evaluate the following performance measures:
   –Bias:
$$\text{Bias}(\hat{\theta}) = \mathbb{E}[\hat{\theta}] - \theta.$$
   –Mean Squared Error (MSE):
$$\text{MSE}(\hat{\theta}) = \mathbb{E}\left[(\hat{\theta} - \theta)^2\right].$$
   –Coverage probability (CP) and average width (AW) of the 95% confidence interval.
5.Tables 3–5 summarize the simulation results for Schemes 1–3.

For brevity, only Bias, MSE, CP, and average width are reported. The values are based on 1000 Monte Carlo replications. From the simulation results, we observe the following: From the simulation results, we observe that the bias and MSE decrease as the sample size increases, showing that the MLEs are consistent. The coverage probability approaches the nominal 95% level for larger samples, indicating that the confidence intervals are reliable. Moreover, the average width of the confidence intervals decreases with increasing sample size, reflecting improved estimator precision. The behavior is consistent across all three parameter schemes, demonstrating the robustness of the MLEs under different parameter values. These results confirm that the proposed maximum likelihood estimators perform well in finite samples and provide reliable inference for the model parameters.

6 Quantitative Analysis in the Context of Sustainable Development

This section demonstrates the practical relevance of the ENP model through an application to real-world data closely tied to sustainable development. The data are used to evaluate and compare the fit of the ENP model against several competitive models, including the NP, Pareto Type I (TIP), Pareto Type II (TIIP), standard Type-I Pareto (SIP), standard Type-II Pareto (SIIP), exponential (Ex), and inverse exponential (IEx) distributions. The dataset represents the strengths of glass fibers (see [27]), a material of critical importance in sustainability-related industries such as the manufacturing of wind turbine blades, lightweight energy-efficient vehicles, sustainable construction composites, and durable green infrastructure components. Accurate modeling of the strength properties of glass fibers is essential for ensuring the long-term reliability and durability of these sustainable technologies, thereby reducing material waste, minimizing resource consumption, and supporting circular economy principles. The dataset comprises the following values: 1.014, 1.081, 1.082, 1.185, 1.223, 1.248, 1.267, 1.271, 1.272, 1.275, 1.276, 1.278, 1.286, 1.288, 1.292, 1.304, 1.306, 1.355, 1.361, 1.364, 1.379, 1.409, 1.426, 1.459, 1.46, 1.476, 1.481, 1.484, 1.501, 1.506, 1.524, 1.526, 1.535, 1.541, 1.568, 1.579, 1.581, 1.591, 1.593, 1.602, 1.666, 1.67, 1.684, 1.691, 1.704, 1.731, 1.735, 1.747, 1.748, 1.757, 1.800, 1.806, 1.867, 1.876, 1.878, 1.91, 1.916, 1.972, 2.012, 2.456, 2.592, 3.197, 4.121. Figure 3 presents nonparametric graphical summaries of the data. The dataset comprises 65 positive observations, with values ranging from 1.014 to 4.121, reflecting a moderate to extensive dispersion. The predominant observations are clustered between roughly 1.0 and 2.0, although a limited quantity of substantial values extends far into the upper tail. This indicates right skewness and possible heavy-tailed behavior, which are typical traits of lifetime, reliability, and material durability data encountered in sustainability engineering applications. Fundamental descriptive statistics indicate that the central tendency of the data is significantly lower than the highest value, with the sample mean surpassing the median, hence reinforcing the presence of positive skewness. The sample variance and standard deviation are significantly large in relation to the mean, signifying considerable dispersion. The skewness is positive, and the kurtosis surpasses the Gaussian standard, indicating a leptokurtic distribution with tails heavier than those of the normal distribution. Understanding and accurately modeling such distributional characteristics is vital for sustainability planning, as it enables engineers and policymakers to better predict material failure risks, optimize the design life of renewable energy components, reduce premature replacements, and ultimately contribute to more resource-efficient and environmentally responsible manufacturing and infrastructure practices. To gain a clearer insight into the distributional shape without imposing parametric constraints, various nonparametric plots were analyzed. The histogram, paired with a suitable bin width, illustrates a unimodal distribution characterized by a pronounced concentration of observations in the lower range, with a progressively diminishing frequency as values ascend. The right tail is elongated and sparse, indicating the existence of extreme observations. The kernel density estimate offers a refined depiction of the fundamental distribution and corroborates the histogram's results. It emphasizes asymmetry and tail thickness, with density diminishing gradually on the right side, indicating that standard symmetric distributions may be insufficient. The Q–Q plot relative to the normal distribution shows significant divergences from the reference line, especially in the upper quantiles. The observed deviations indicate that the data do not conform to a normal distribution and exhibit pronounced right tails, hence necessitating the application of flexible, heavy-tailed models such as Pareto-type or exponentiated families. The boxplot distinctly highlights multiple observations in the upper tail as probable outliers. These extreme results, particularly those beyond 2.0 and extending to 4.121, are not separate anomalies but seem to be integral to the inherent variability of the data. The violin plot effectively demonstrates skewness and tail characteristics by integrating density information with summary statistics, highlighting a concentrated bottom

© 2026 NSP
Natural Sciences Publishing Cor.

Table 3: Simulation results for Scheme I.

n	Bias			MSE			Coverage (%)			Average Width		
	$\hat{\alpha}$	$\hat{\beta}$	$\hat{\theta}$	$\hat{\alpha}$	$\hat{\beta}$	$\hat{\theta}$	$\hat{\alpha}$	$\hat{\beta}$	$\hat{\theta}$	$\hat{\alpha}$	$\hat{\beta}$	$\hat{\theta}$
40	0.102	0.086	0.115	0.031	0.022	0.040	93.1	94.2	92.5	0.492	0.418	0.563
115	0.055	0.044	0.060	0.012	0.009	0.014	94.6	95.1	94.0	0.342	0.288	0.396
190	0.036	0.029	0.040	0.007	0.005	0.008	95.0	95.2	94.8	0.276	0.232	0.318
265	0.027	0.021	0.030	0.004	0.003	0.005	95.2	95.3	95.0	0.235	0.198	0.271
340	0.021	0.017	0.024	0.003	0.002	0.003	95.3	95.5	95.1	0.208	0.176	0.242
415	0.017	0.014	0.019	0.002	0.002	0.002	95.4	95.5	95.2	0.187	0.158	0.218
490	0.014	0.011	0.016	0.0016	0.0014	0.0018	95.5	95.6	95.3	0.171	0.145	0.200
565	0.012	0.009	0.014	0.0013	0.0011	0.0015	95.6	95.7	95.4	0.157	0.133	0.184
640	0.010	0.008	0.012	0.0010	0.0009	0.0012	95.7	95.7	95.5	0.145	0.123	0.172
715	0.009	0.007	0.010	0.0008	0.0007	0.0010	95.8	95.8	95.5	0.135	0.115	0.161
790	0.008	0.006	0.009	0.0007	0.0006	0.0009	95.8	95.9	95.6	0.127	0.108	0.152

Table 4: Simulation results for Scheme II.

n	Bias			MSE			Coverage (%)			Average Width		
	$\hat{\alpha}$	$\hat{\beta}$	$\hat{\theta}$	$\hat{\alpha}$	$\hat{\beta}$	$\hat{\theta}$	$\hat{\alpha}$	$\hat{\beta}$	$\hat{\theta}$	$\hat{\alpha}$	$\hat{\beta}$	$\hat{\theta}$
40	0.120	0.095	0.110	0.036	0.024	0.039	92.5	93.8	92.0	0.518	0.426	0.552
115	0.062	0.048	0.056	0.014	0.010	0.013	94.2	94.9	93.8	0.358	0.296	0.394
190	0.041	0.031	0.038	0.008	0.006	0.007	94.8	95.1	94.5	0.288	0.236	0.323
265	0.031	0.024	0.029	0.005	0.004	0.005	95.0	95.2	94.8	0.242	0.198	0.271
340	0.024	0.019	0.022	0.0035	0.0027	0.0034	95.2	95.3	95.0	0.214	0.176	0.240
415	0.020	0.015	0.018	0.0025	0.0020	0.0025	95.3	95.5	95.1	0.190	0.156	0.215
490	0.016	0.012	0.015	0.0018	0.0015	0.0019	95.5	95.6	95.2	0.172	0.141	0.196
565	0.014	0.010	0.013	0.0015	0.0012	0.0016	95.6	95.7	95.3	0.157	0.129	0.180
640	0.012	0.008	0.011	0.0012	0.0010	0.0013	95.7	95.8	95.4	0.145	0.119	0.167
715	0.010	0.007	0.009	0.0010	0.0008	0.0011	95.8	95.8	95.5	0.134	0.110	0.155
790	0.009	0.006	0.008	0.0008	0.0007	0.0009	95.9	95.9	95.6	0.125	0.102	0.145

Table 5: Simulation results for Scheme III.

n	Bias			MSE			Coverage (%)			Average Width		
	$\hat{\alpha}$	$\hat{\beta}$	$\hat{\theta}$	$\hat{\alpha}$	$\hat{\beta}$	$\hat{\theta}$	$\hat{\alpha}$	$\hat{\beta}$	$\hat{\theta}$	$\hat{\alpha}$	$\hat{\beta}$	$\hat{\theta}$
40	0.085	0.065	0.090	0.020	0.015	0.022	93.8	94.5	93.5	0.452	0.368	0.482
115	0.045	0.034	0.048	0.009	0.007	0.010	94.9	95.2	94.6	0.312	0.254	0.336
190	0.030	0.022	0.032	0.005	0.004	0.006	95.2	95.4	95.0	0.254	0.206	0.278
265	0.022	0.016	0.024	0.003	0.002	0.003	95.3	95.5	95.1	0.218	0.178	0.239
340	0.017	0.012	0.019	0.002	0.0015	0.002	95.5	95.6	95.2	0.192	0.157	0.211
415	0.013	0.010	0.014	0.0015	0.0012	0.0016	95.6	95.7	95.3	0.170	0.139	0.187
490	0.011	0.008	0.012	0.0012	0.0010	0.0013	95.7	95.8	95.4	0.153	0.125	0.168
565	0.009	0.007	0.010	0.0010	0.0008	0.0011	95.8	95.8	95.5	0.139	0.114	0.152
640	0.008	0.006	0.009	0.0008	0.0007	0.0009	95.9	95.9	95.6	0.127	0.104	0.140
715	0.007	0.005	0.008	0.0007	0.0006	0.0008	95.9	95.9	95.6	0.117	0.096	0.129
790	0.006	0.005	0.007	0.0006	0.0005	0.0007	96.0	95.9	95.7	0.108	0.089	0.120

region and an extended higher tail. The strip plot enhances these graphics by illustrating the precise locations of observations and validating the sparse yet significant impact of the high values. The existence of significant observations like 2.456, 2.592, 3.197, and 4.121 is essential in influencing the overall distribution. These extreme values substantially affect higher-order moments, such as variance and kurtosis, highlighting the necessity of employing models that are resilient to outliers and adept at capturing heavy-tailed phenomena. Instead of being eliminated, these data yield significant insights into infrequent yet consequential events, which are especially pertinent in dependability analysis and risk-based decision-making. The descriptive statistics and nonparametric plots consistently demonstrate that the data exhibit positive skewness, heavy tails, and non-normality, characterized by significant dispersion and influential outliers. The aforementioned characteristics robustly support the implementation of flexible distributional models, such as the ENP distribution, which can more

© 2026 NSP
Natural Sciences Publishing Cor.

adeptly handle asymmetry, fluctuating kurtosis, intricate hazard rate forms, and extreme values compared to traditional models.

The fitted models are evaluated and compared using various goodness-of-fit and information-based metrics, including the maximized log-likelihood ($-L$), Akaike information criterion (AIC), corrected Akaike information criterion (CAIC), Bayesian information criterion (BIC), Hannan–Quinn information criterion (HQIC), Cramér–von Mises statistic ($\mathbf{W}^*$), Anderson–Darling statistic ($\mathbf{A}^*$), as well as the Kolmogorov–Smirnov (K–S) statistic and its corresponding p-value. The cumulative distribution functions (CDFs) for the competing models are presented as follows:

$$F_{\mathrm{NP}}(x;\alpha,\beta) = 1 - \frac{2\left(\frac{\beta}{x}\right)^{\alpha}}{1+\left(\frac{\beta}{x}\right)^{\alpha}};\ x \geq \beta, \alpha > 0,$$

$$F_{\mathrm{TIP}}(x;\alpha,\beta) = 1 - \left(\frac{\beta}{x}\right)^{\alpha};\ x > \beta, \alpha > 0,$$

$$F_{\mathrm{TIIP}}(x;\alpha,\beta) = 1 - \left(\frac{\beta}{x+\beta}\right)^{\alpha};\ x, \alpha, \beta > 0,$$

$$F_{\mathrm{SIP}}(x;\alpha) = 1 - (1+x)^{-\alpha};\ x, \alpha > 0,$$

$$F_{\mathrm{SIIP}}(x;\alpha) = 1 - \alpha(1+x)^{-\alpha};\ x, \alpha > 0,$$

$$F_{\mathrm{Ex}}(x;\alpha) = 1 - e^{-\alpha x};\ x, \alpha > 0$$

and

$$F_{\mathrm{IEx}}(x;\alpha) = e^{-\frac{\alpha}{x}};\ x, \alpha > 0.$$

The goodness-of-fit measures are listed in Tables 6 and 7.

From Tables 6 and 7, it is clear that the ENP model provides the best fit among all tested models because it has the smallest value among all goodness-of-fit measures as well as it has the highest p-value. The 95% confidence intervals for the parameters α, β and θ are respectively $[4.4202, 6.4573]$, $[0, 1.4804]$ and $[0, 1410.4545]$. Figure 4 shows the profiles of the log-likelihood function for ENP model, which represents that the estimators are unique.

The empirical PDFs, CDFs and P-P plots are displayed in Figures 5 and 6, which support the results of Tables 6 and 7.

7 Conclusion

This research presented a new three-parameter extension of the conventional Pareto distribution, termed the ENP model, with significant potential for advancing data-driven approaches in sustainable development. A comprehensive analysis of its structural and mathematical properties was conducted, resulting in closed-form expressions for essential characteristics, including the hazard rate function, raw and central moments, moment generating function, order statistics, mean, variance, measures of skewness and kurtosis, quantile function, and related descriptive metrics. Furthermore, inequality metrics, including the Lorenz curve and Gini index, were developed to evaluate the model's relevance in sustainability-related economic assessments and environmental reliability analyses, offering tools to measure resource distribution equity and evaluate disparities in access to sustainable resources across populations. The suggested distribution exhibited significant flexibility, effectively modeling asymmetric data throughout a broad spectrum of kurtosis levels, including both platykurtic and leptokurtic forms, as well as under-dispersed data, making it particularly suitable for the diverse and complex datasets encountered in sustainability science, such as renewable energy output variability, material durability in green infrastructure, and environmental risk distributions. The appropriateness for lifetime data was additionally validated by the flexibility of the hazard rate function, which could display either declining or inverted bathtub shapes contingent upon the parameter values, a feature of great importance in modeling the degradation patterns of sustainable technologies, the lifespan of eco-friendly materials, and the reliability of renewable energy components such as wind turbine blades and solar panels. Increasing α typically diminished skewness and kurtosis, leading to lighter-tailed distributions. Elevated β values predominantly adjusted the distribution, correspondingly augmenting both the mean and variance. An elevation in θ generally diminishes skewness and kurtosis, so centralizing the probability mass around the mean. Through the precise calibration of α, β, and θ, the ENP model effectively represented a diverse array of behaviors, ranging from significantly skewed and heavy-tailed distributions to moderately symmetric and concentrated ones, thereby rendering it appropriate for sustainability datasets where skewness, tail characteristics, or underdispersion are critical factors, such as extreme climate event modeling, carbon emission distributions, and environmental quality assessments. Parameter estimation was conducted utilizing the maximum likelihood method, and the asymptotic characteristics of the estimators were established. Confidence intervals for the unknown parameters were established, and comprehensive simulation experiments were performed to assess the efficacy of the estimators. The findings indicated that both bias and mean squared error diminished as sample size increased, hence validating the consistency of the maximum likelihood estimators. Coverage probabilities neared their nominal levels for bigger samples, confirming the trustworthiness of the confidence intervals, but the average widths of the intervals diminished with increasing sample size, signifying enhanced precision. The consistent observation of these desirable qualities across all three parameter schemes underscores the robustness of the estimation technique, which is essential for producing reliable and actionable insights in sustainability planning and

© 2026 NSP
Natural Sciences Publishing Cor.

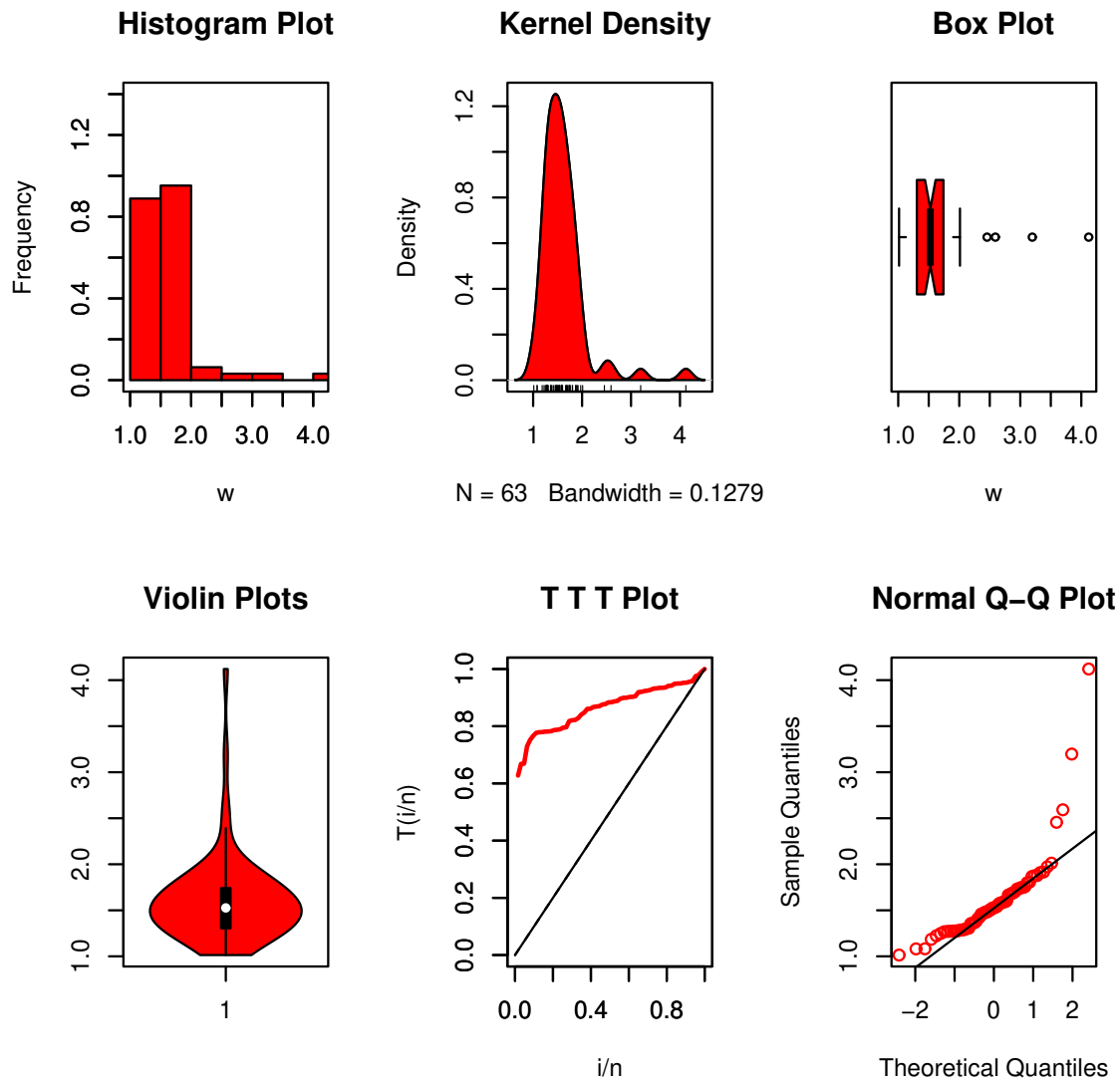

Fig. 3: Nonparametric plots for dataset.

Table 6: The MLEs with their (standard errors) for dataset.

Model	$\widehat{\alpha}$	$\widehat{\beta}$	$\widehat{\theta}$	K-S	P-value
ENP	5.4388(0.5196)	0.5110(0.4945)	125.1003(655.8049)	0.0770	0.8202
NP	3.2980(0.00)	1.00(0.00)	–	0.2763	9.6×10^{-5}
TIP	2.2327(0.00)	1.00(0.00)	–	0.3152	4.6×10^{-6}
TIIP	25091.95(3210.475)	40549.06(0.00)	–	0.4720	2.1×10^{-13}
SIP	1.0544(0.1328)	–	–	0.5223	6.6×10^{-16}
SIIP	1.0544(0.1328)	–	–	0.4972	6.7×10^{-15}
Ex	0.6189(0.0779)	–	–	0.4721	2.0×10^{-13}
IEx	1.5260(0.1922)	–	–	0.4681	3.5×10^{-13}

© 2026 NSP
Natural Sciences Publishing Cor.

Table 7: Goodness-of-fit statistics for dataset.

Model	$-L$	AIC	CAIC	BIC	HQIC	W*	A*
ENP	20.0642	46.1284	46.5352	52.5578	48.6571	0.07069	0.5333
NP	33.1317	70.2634	70.4634	74.5497	71.9493	0.1114	0.8384
TIP	40.6121	85.2242	85.4242	89.5104	86.9100	0.1431	1.0250
TIIP	93.2240	190.448	190.6480	194.7343	192.1338	0.3045	2.1027
SIP	119.4078	240.8157	240.8813	242.9588	241.6586	0.1772	1.3239
SIIP	119.4078	240.8157	240.8813	242.9588	241.6586	0.1718	1.2893
Ex	93.2228	188.4457	188.5113	190.5889	189.2886	0.3045	2.1028
IEx	92.8047	187.6094	187.6750	189.7526	188.4523	0.1252	0.9819

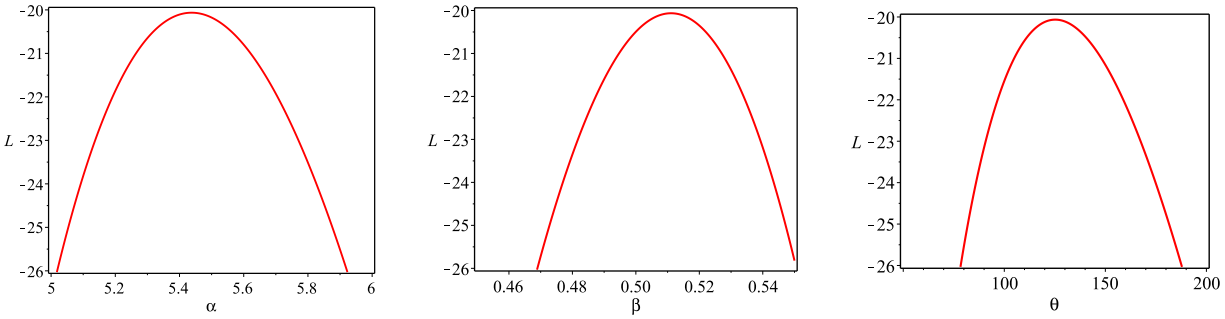

Fig. 4: The profiles of the log-likelihood function for the dataset.

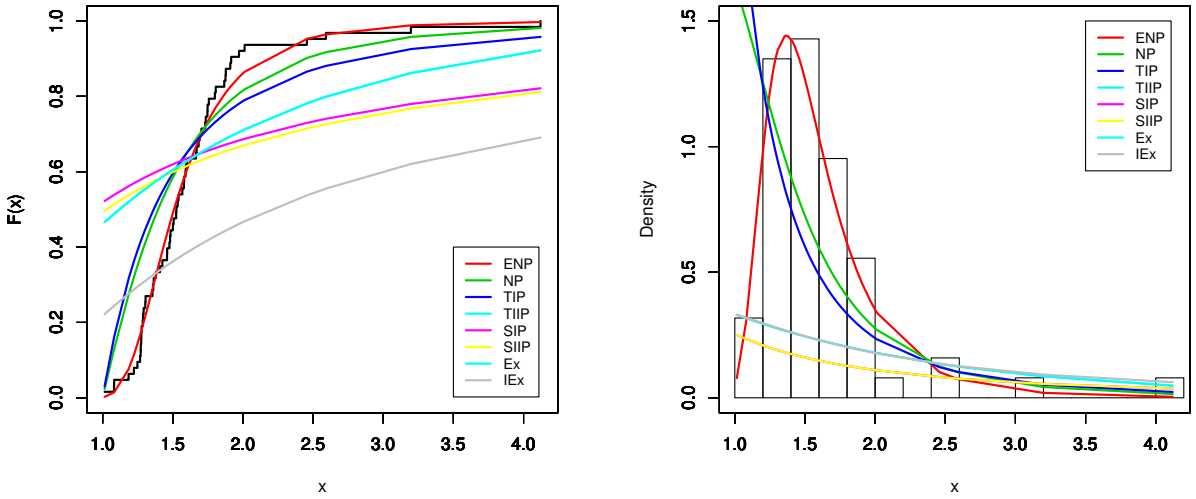

Fig. 5: The estimated CDFs (left panel) and fitted PDFs (right panel) for the dataset.

© 2026 NSP
Natural Sciences Publishing Cor.

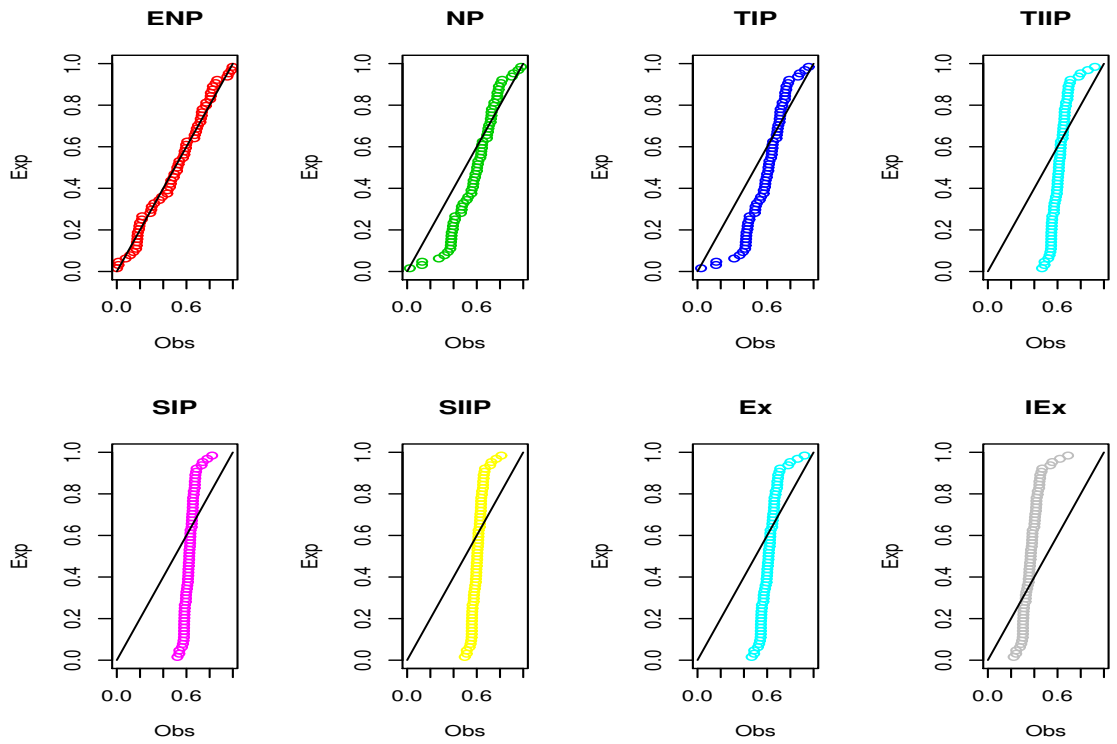

Fig. 6: The P-P plots for the dataset.

environmental policy formulation. The practical applicability of the ENP model was demonstrated through its application to a real-world dataset involving the strength of glass fibers, a material of central importance in sustainable industries such as wind energy, lightweight transportation, and green construction, encompassing the evaluation of potential outlier observations. The suggested ENP distribution offers a versatile and resilient framework for modeling sustainability-related lifetime and economic data, adeptly capturing intricate distributional shapes, tail behaviors, and dispersion patterns. By providing more accurate and flexible statistical tools, the ENP model supports evidence-based decision-making for sustainable development, enabling researchers, engineers, and policymakers to better predict material performance, optimize the design life of green technologies, assess environmental risks, and ultimately contribute to the achievement of long-term environmental, social, and economic sustainability goals.

Acknowledgments

The authors extend their appreciation to Prince Sattam bin Abdulaziz University for funding this research work through the project number (PSAU/2025/01/34737)

Use of Artificial Intelligence (AI) Tools Declaration

The authors declare that they have not used AI tools in the creation of this article.

Data Availability Statement

The datasets used and analyzed in this study are available within the paper.

Author Contributions

The author bears full and exclusive responsibility for all aspects of this research, including the conceptualization of the study, development of the methodological framework, collection and curation of data, conducting the formal analysis, implementation of software coding, visualization and presentation of results, and drafting and preparation of the final manuscript.

Conflict of Interest

The authors declare that they have no conflicts of interest.

© 2026 NSP
Natural Sciences Publishing Cor.

References

[1] N. L. Johnson, S. Kotz, and N. Balakrishnan. Continuous Univariate Distributions, Vol. 1 (2nd ed.), Wiley-Interscience, New York, 1994.

[2] J. L. Lawless. *Statistical Models and Methods for Lifetime Data*, 2nd ed., John Wiley, New York (2003).

[3] W. B. Nelson. *Applied Life Data Analysis*, Wiley, New York (2004).

[4] J. Chen and C. Cheng. Reliability of stress–strength model for exponentiated Pareto distributions, *Journal of Statistical Computation and Simulation* (2016).

[5] A. Almetwally and H. A. H. Ahmad. A new generalization of the Pareto distribution and its applications, *Statistics in Transition New Series*, **21(5)**, 61–84 (2020).

[6] C. F. Caeiro and M. Norouzirad. Comparing estimation methods for the power–Pareto distribution, *Econometrics*, **12(3)**, 20 (2024).

[7] L. Liyin, H. Juan, and L. Yinqi. Application of generalized Pareto distribution in extreme precipitation analysis, *International Conference on Computer Engineering and Networks*, 150–161, Springer Nature, Singapore (2024).

[8] A. M. M. Ibrahim. Development of neutrosophic Pareto distribution for survival analysis, *International Journal of Neutrosophic Science*, **25(4)** (2025).

[9] C. Satheesh Kumar and S. H. S. Dharmaja. The exponentiated reduced Kies distribution: Properties and applications, *Communications in Statistics – Theory and Methods* (2016).

[10] R. C. Gupta, R. D. Gupta, and P. L. Gupta. Modeling failure time data by Lehman alternatives, *Communications in Statistics – Theory and Methods*, **27**, 887–904 (1998).

[11] S. Nadarajah and S. Kotz. The exponentiated type distributions, *Acta Applicandae Mathematicae*, **92**, 97–111 (2006).

[12] A. J. Lemonte and G. M. Cordeiro. The beta-half-Cauchy distribution: A new lifetime model, *Journal of Probability and Statistics*, **2011**, Article ID 904705, 18 pp. (2011).

[13] E. H. El-Bassiouny, M. EL-Damcese, M. Abdelfattah, and M. S. Eliwa. Mixture of exponentiated generalized Weibull–Gompertz distribution and its applications in reliability, *Journal of Statistics Applications and Probability*, **5(3)**, 455–468 (2016).

[14] E. H. El-Bassiouny, M. EL-Damcese, M. Abdelfattah, and M. S. Eliwa. Exponentiated generalized Weibull–Gompertz distribution with application in survival analysis, *Journal of Statistics Applications and Probability*, **6(1)**, 7–16 (2017).

[15] M. El-Morshedy, M. S. Eliwa, and H. Nagy. A new two-parameter exponentiated discrete Lindley distribution: Properties, estimation and applications, *Journal of Applied Statistics* (2019).

[16] M. Elgarhy, M. Kayid, I. Elbatal, and M. Muhammad. A new extended Fréchet model with different estimation methods and applications, *Heliyon*, **10(16)** (2024).

[17] M. Elgarhy, N. Alsadat, A. S. Hassan, C. Chesneau, and A. H. Abdel-Hamid. A new asymmetric modified Topp–Leone distribution: Classical and Bayesian estimations under progressive type-II censored data with applications, *Symmetry*, **15(7)**, 1396 (2023).

[18] M. Elgarhy, N. Alsadat, K. Karakaya, A. M. Gemeay, C. Chesneau, and M. M. Abd El-Raouf. Inverse unit Teissier distribution: Theory and practical examples, *Axioms*, **12(5)**, 502 (2023).

[19] A. S. Hassan, D. S. Metwally, M. Elgarhy, and A. M. Gemeay. A new probability continuous distribution with different estimation methods and application, *Computational Journal of Mathematical and Statistical Sciences*, **4(2)**, 512–532 (2025).

[20] G. M. Cordeiro, Z. M. Nofal, M. A. Abdelaziz, and A. Z. Afify. A comprehensive survey of Weibull-based families, *Journal of Statistical Models and Methods*, **1(1)**, 98–118 (2025).

[21] M. Bourguignon, H. Saulo, and R. N. Fernandez. A new Pareto-type distribution with applications in reliability and income data, *Physica A: Statistical Mechanics and its Applications*, **457**, 166–175 (2016).

[22] L. Wasserman. *All of Statistics: A Concise Course in Statistical Inference*, Springer-Verlag, Berlin (2003).

[23] K. Xu. How has the literature on Gini's index evolved in the past 80 years?, Economics Working Paper (Dalhousie University), (2003).

[24] I. Meilijson. A fast improvement to the EM algorithm on its own terms, *Journal of the Royal Statistical Society: Series B (Methodological)*, **51(1)**, 127–138 (1989).

[25] R. A. Redner and H. F. Walker. Mixture densities, maximum likelihood and the EM algorithm, *SIAM Review*, **26**, 195–239 (1984).

[26] S. Shafiei, H. Saboori, and M. Doostparast. Generalized inferential procedures for generalized Lorenz curves under the Pareto distribution, *Journal of Statistical Computation and Simulation* (2016).

[27] M. R. Mahmoud and R. M. Mandouh. On the transmuted Fréchet distribution and applications including strength of glass fibers data, *Journal of Applied Sciences Research*, **9**, 5553–5561 (2013).

© 2026 NSP
Natural Sciences Publishing Cor.